NASA TECHNICAL NOTE

NASA TN D-7635

NASA TN D-7635

DIFFERENTIAL ANALYSIS FOR THE TURBULENT BOUNDARY LAYER ON A COMPRESSOR BLADE ELEMENT (INCLUDING BOUNDARY-LAYER SEPARATION)

by James F. Schmidt and Carroll A. Todd

Lewis Research Center
Cleveland, Ohio 44135

NATIONAL AERONAUTICS AND SPACE ADMINISTRATION • WASHINGTON, D. C. • APRIL 1974

1. Report No.	2. Government Accession No.	3. Recipient's Catalog No.
NASA TN D-7635		

4. Title and Subtitle	5. Report Date
DIFFERENTIAL ANALYSIS FOR THE TURBULENT BOUNDARY LAYER ON A COMPRESSOR BLADE ELEMENT (INCLUDING BOUNDARY-LAYER SEPARATION)	APRIL 1974
	6. Performing Organization Code

7. Author(s)	8. Performing Organization Report No.
James F. Schmidt and Carroll A. Todd	E-7506
	10. Work Unit No. 501-24

9. Performing Organization Name and Address	11. Contract or Grant No.
Lewis Research Center National Aeronautics and Space Administration Cleveland, Ohio 44135	
	13. Type of Report and Period Covered: Technical Note

12. Sponsoring Agency Name and Address	14. Sponsoring Agency Code
National Aeronautics and Space Administration Washington, D.C. 20546	

15. Supplementary Notes

16. Abstract

A two-dimensional differential analysis is developed to approximate the turbulent boundary layer on a compressor blade element with strong adverse pressure gradients, including the separated region with reverse flow. The predicted turbulent-boundary-layer thicknesses and velocity profiles are in good agreement with experimental data for a cascade blade, even in the separated region.

17. Key Words (Suggested by Author(s))

Fluid mechanics; Turbulent boundary layer; Separated turbulent boundary layer; High turbulence levels; Compressor blade element

18. Distribution Statement

Unclassified - unlimited

Cat. 12

19. Security Classif. (of this report)	20. Security Classif. (of this page)	21. No. of Pages	22. Price*
Unclassified	Unclassified	29	$3.25

* For sale by the National Technical Information Service, Springfield, Virginia 22151

DIFFERENTIAL ANALYSIS FOR THE TURBULENT BOUNDARY LAYER ON A COMPRESSOR BLADE ELEMENT (INCLUDING BOUNDARY-LAYER SEPARATION)

by James F. Schmidt and Carroll A. Todd

Lewis Research Center

SUMMARY

In order to provide an approximate boundary-layer prediction at the trailing edge of a compressor blade (especially with separated flow), a two-dimensional differential analysis is developed for the turbulent boundary layer (including the separated reverse-flow region). Prandtl's classical mixing-length theory is used with a single eddy-diffusivity model throughout the boundary-layer region. The use of a new shear-stress function (instead of a velocity function) for the dependent variable in the momentum equation makes it possible to calculate mathematically stable solutions into the boundary-layer separation region.

This analysis is applied to a blade in a cascade with three different inlet-flow angles for comparison with experimental boundary-layer measurements. The predicted turbulent-boundary-layer thicknesses and velocity profiles are in good agreement with experimental data, even in the separated region. For the thickest turbulent boundary layer on the blade with a separated region, 8 minutes of computing time (Lewis DCS 7094-7044) are necessary for this calculation.

INTRODUCTION

In the analysis of compressor blade performance, many basic flow parameters such as maximum blade loading, blade loss, and blade stall are primarily related to the blade-surface boundary layer. Therefore, the need exists for a boundary-layer calculation procedure to aid in the blade-row flow analysis, especially in the flow-separation region. To select or develop a suitable boundary-layer calculation technique, some characteristics of the flow through compressor blade rows must be known.

All compressor blade rows are designed to increase the static pressure of the fluid. Thus, the blade-surface boundary layer experiences an adverse pressure gradient. With high blade loading and near-stall operation, these adverse pressure gradients become very strong and a separated boundary-layer flow region often occurs.

In general, the airflow entering the blade rows is very turbulent (high turbulence intensity level) because it has passed through an upstream blade row and a long inlet. The shear wakes from the upstream blade row and the strong adverse-pressure-gradient flow history produce a flow environment of high free-stream turbulence intensity.

Over much of their operating ranges, compressor blades produce large velocity peaks very close to the nose of the blade (on the suction surface). And thereby, adverse pressure gradients are expected over almost the entire length of the blade. These strong adverse pressure gradients (shortly after the leading edge of the blade), as well as high turbulence intensity levels, tend to cause early transition or separation and reattachment as a turbulent boundary layer. Therefore, the turbulent boundary layer effectively exists over the entire blade. Hence, a theoretical analysis is needed which can calculate the turbulent boundary layer (with high turbulence intensity levels) through the blade stall flow-separation region. However, a turbulent-boundary-layer calculation in the separated flow region is not only mathematically very difficult but also depends upon the unknown and unmeasured Reynolds turbulent shear stress. Thus, this boundary-layer prediction must be considered an approximation.

In the past, either a turbulent-boundary-layer growth correlation or, more recently, an integral boundary-layer analysis (ref. 1) was used to predict the boundary-layer growth on a compressor blade element. Most integral analyses, however, do not have the capability of predicting the boundary-layer growth in the separated reverse-flow region.

In addition, several differential numerical calculation methods have been developed for the turbulent boundary layer (refs. 2 to 6). All these calculation methods use an eddy-diffusivity concept for the unknown turbulent Reynolds shear stress and a finite-difference calculation procedure which utilizes a velocity function as the prime dependent variable across the boundary layer. Considering that the velocity profile will have an inflection point at and beyond the separation point, the authors believe the use of a velocity function as the prime dependent variable may cause large numerical errors and instabilities in the basic finite-difference differentiation technique.

Presently, very few analytical methods are available for calculating turbulent separated flows caused by adverse pressure gradients. One such method (ref. 7) presents an integral turbulent-boundary-layer analysis which was applied to turbulent flows near and in the separated region. However, a comparison of the integral analysis of reference 7 with experimental data (near and in the separated region) still shows considerable discrepancies in the boundary-layer thicknesses (ref. 7). In all these

turbulent-boundary-layer analyses (refs. 1 to 7), the free-stream turbulence level is assumed to be small; and this, in general, is not indicative of the boundary-layer flow over compressor blades.

This report develops an analysis for the turbulent boundary layer on compressor blades, including the separated region with reverse flow. The present two-dimensional analysis is a successive-approximation, nonsimilar calculation (as in ref. 8) of the turbulent, differential, boundary-layer equations. The calculation system of the present analysis is suitable for calculating the turbulent boundary layer in strong adverse-pressure-gradient regions and also in reverse-flow separated regions. The use of a new shear-stress function for the dependent variable in the momentum equation makes it possible to calculate mathematically stable solutions into the separated region.

At the separation point and in the reverse-flow separated region, even the complete boundary-layer equations (ref. 9) may not be valid. In addition, the eddy diffusivity is presently unknown in the separated boundary-layer region. Also, the momentum equation normal to the blade surface is not included in the present system of boundary-layer equations, and the pressure is assumed to be constant across the boundary layer. For these reasons, the present turbulent-boundary-layer solutions in the separated flow region should be considered an engineering approximation.

The present analysis also uses the eddy-diffusivity concept for the unknown turbulent Reynolds shear stress, but with a different eddy-diffusivity model than those used in previous analyses. Since high free-stream turbulence levels as well as extreme, adverse pressure gradients are characteristic of flows over compressor blades, a large free-stream shear flow is believed to describe the rotational inviscid flow over compressor blades. Thereby, the large shear stress in the turbulent boundary layer does not diminish to the usual insignificant value at the edge of the boundary layer. In fact, the shear stress at the edge of the blade turbulent boundary layer is assumed in this analysis to be a large significant fraction of the maximum shear stress in the boundary layer. This large-shear-stress behavior at the edge of the boundary layer has experimentally been measured in a turbulent boundary layer with high levels of free-stream turbulence intensity (ref. 10). Based on these reasons, Prandtl's mixing-length theory (ref. 9) for the eddy diffusivity, with Van Driest's damping factor (ref. 11), is used throughout the entire boundary layer.

The results of this analysis are compared with the experimental turbulent-boundary-layer measurements of reference 12. Reference 12 gives two- and three-dimensional, turbulent-boundary-layer measurements on a blade in a cascade for several inlet-flow angles. These measurements include the turbulent-boundary-layer, flow-separation region. The turbulence intensity level for this cascade flow is reported to be high (ref. 12).

ANALYSIS

The present analysis is a nonsimilar differential calculation of the turbulent-boundary-layer equations.

Assumptions

The analysis is based on the following assumptions:

(1) Surface curvature is neglected in the boundary-layer equations.

(2) Flow is two dimensional and steady.

(3) Normal Reynolds stresses are negligible, even for reverse flow.

(4) Static pressure is constant across the boundary layer.

(5) The eddy-diffusivity concept can be used for the tangential Reynolds shear stress.

(6) Prandtl's eddy-diffusivity, mixing-length theory is assumed to be applicable for the turbulent boundary layer on blade surfaces with very strong, adverse pressure gradients and high turbulence levels.

(7) The eddy diffusivity is always positive, even for reverse flow.

(8) The turbulent boundary layer begins at the stagnation point on the blade surface.

Basic Equations

In reference 8, the turbulent-boundary-layer equations for axisymmetric steady flow are presented in terms of the eddy-diffusivity concept. For two-dimensional flow, the system of boundary-layer equations in reference 8 reduces to

Continuity:

$$(\rho U)_S + (\rho V)_S = 0 \tag{1}$$

Momentum:

$$\rho U U_S + \rho V U_y = \rho_e U_e (U_e)_S + \left[(\mu + \rho\epsilon) U_y\right]_y \tag{2}$$

Energy:

$$\rho U H_S + \rho V H_y = \left[\left(\frac{\mu}{Pr_L} + \frac{\rho\epsilon}{Pr_T}\right) H_y\right] + \left[\mu\left(1 - \frac{1}{Pr_L}\right)\left(\frac{U^2}{2}\right)_y\right]_y \tag{3}$$

State:

$$P = \rho \mathcal{R} t \tag{4}$$

(All symbols are defined in appendix A.)

The boundary-layer coordinate system along a blade cross section is shown in figure 1, where S is the boundary-layer coordinate parallel to the blade surface, c is the chord length, x is the distance coordinate from the nose to the trailing edge of the airfoil section, and x/c is the percentage-of-chord location (0 to 100).

Eddy-Diffusivity Model

Before the turbulent-boundary-layer equations (1) to (4) can be solved, an expression for the eddy diffusivity ϵ is needed. As discussed in the INTRODUCTION, a one-layer model is assumed for the eddy diffusivity. The eddy diffusivity is given by Van Driest's modification (ref. 11) (viscous damping effect near the wall) of Prandtl's mixing-length expression (ref. 2):

$$\epsilon = \kappa^2 y^2 \left|\frac{\partial U}{\partial y}\right| \left(1 - \frac{1}{e^{y/A}}\right)^2 \tag{5}$$

where A is (from ref. 2)

$$A = 26 \frac{\mu_w}{\rho_w} \left(\frac{\rho_w}{\tau_w}\right)^{1/2} \tag{6}$$

and κ is an experimental flow constant (0.40) based on low-speed incompressible data. The dynamic viscosity of air is approximated by

$$\mu = \mu_0 \left(\frac{t}{T_0}\right)^d \tag{7}$$

Transformed Equations

Using a compressibility type of transformation (ref. 13) yields the following transformation equations, used in solving the boundary-layer equations (1) and (2):

$$\eta = \frac{\rho_e (U_e)^{1/2}}{(\rho_0 \mu_0 2S)^{1/2}} \int_0^y \frac{\rho}{\rho_e} \, dy \tag{8a}$$

$$\bar{S} = S \tag{8b}$$

The partial derivatives transform as follows:

$$( )_y = \frac{\rho U_e^{1/2}}{(\rho_0 \mu_0 2\bar{S})^{1/2}} ( )_\eta + ( )_{\bar{S}} \bar{S}_y \qquad \bar{S}_y = 0 \tag{8c}$$

$$( )_S = ( )_{\bar{S}} + ( )_\eta \eta_S \tag{8d}$$

From continuity, the stream function ψ is defined such that

$$\rho U = (\psi)_y \tag{8e}$$

$$\rho V = -(\psi)_S \tag{8f}$$

By letting

$$\psi = \left(\rho_0 \mu_0 2\bar{S} U_e\right)^{1/2} f(\eta, \bar{S}) \tag{8g}$$

Then,

$$f_\eta = \frac{U}{U_e} \tag{8h}$$

Applying the transformation equations (8) to the momentum equation (2) and reducing give the following form for the momentum equation:

$$\left\{\left[C + D_1\left(\frac{\rho}{\rho_e}\right)^2 \epsilon\right] f_{\eta\eta}\right\}_\eta + (fD_2 + 2\bar{S}f_{\bar{S}})f_{\eta\eta} = 2\bar{S}f_\eta\left(f_\eta\right)_{\bar{S}} - \beta\left[\frac{1}{\frac{\rho}{\rho_e}} - (f_\eta)^2\right] \tag{9}$$

where the parameters in equation (9) are as follows: the density-viscosity ratio C is defined as

$$C = \frac{\rho\mu}{\rho_0\mu_0} = \frac{P_e}{P_0}\frac{T_0}{t}\frac{\mu}{\mu_0} \tag{10}$$

Using equations (7) and (8f) with the definition of total temperature

$$T = t + \frac{U^2}{2c_p}$$

in equation (10) and reducing result in the transformed density-viscosity ratio

$$C = \frac{P_e}{P_0}\left[\frac{1}{1 - D_3(f_\eta)^2}\right]^{1-d} \tag{11}$$

and the ratio of kinetic to total energy

$$D_3 = \frac{U_e^2}{2c_pT_0} \tag{12}$$

The density ratio ρ/ρ_e can be expressed as

$$\frac{\rho}{\rho_e} = \frac{t_e}{t} = \frac{1 - D_3}{1 - D_3(f_\eta)^2} \tag{13}$$

The flow coefficients D_1 and D_2 are

$$D_1 = \frac{\rho_e^2}{\rho_0 \mu_0} \tag{14}$$

$$D_2 = 1 + \frac{\beta}{2} \tag{15}$$

where the velocity gradient parameter β is

$$\beta = \frac{2\bar{S}}{U_e}\left(U_e\right)_{\bar{S}} \tag{16}$$

And $\bar{S}$ is the boundary-layer distance coordinate starting at the origin of the turbulent boundary layer.

In the momentum equation (9), the terms involving the velocity derivatives with respect to $\bar{S}$, $2\bar{S}f_{\bar{S}}f_{\eta\eta}$, and $2\bar{S}f_{\eta}\left(f_{\eta}\right)_{\bar{S}}$ are the nonsimilar terms that were neglected in the similar-solution calculation of reference 8. The energy equation is transformed and programmed in the computer program but is not indicated in the present analysis. This omission is believed to result in a less complex presentation of the theory, especially since the test cases do not include energy transfer.

With substitution of the transformation equations (8) into equations (5) to (7) and reduction, the transformed eddy diffusivity becomes

$$\epsilon = \kappa^2 \frac{\rho}{\rho_e} \frac{\left(\rho_0 \mu_0 2\bar{S} U_e\right)^{1/2}}{\rho_e} \left|f_{\eta\eta}\right| \left[\int_0^{\eta} \frac{d\eta}{\frac{\rho}{\rho_e}}\right]^2 \left(1 - \frac{1}{e^{y^+/26}}\right)^2 \tag{17}$$

where y^+ is given by

$$y^+ = \frac{y\left(\frac{\tau_w}{\rho_w}\right)^{1/2}}{\frac{\mu_w}{\rho_w}} = \frac{yU_e}{\frac{\mu_w}{\rho_w}} \left(\frac{C_f}{2} \frac{\rho_e}{\rho_w}\right)^{1/2} \tag{18}$$

Grouping the molecular viscosity and eddy diffusivity into one coefficient gives

$$\overline{C}_1 = C + D_1\left(\frac{\rho}{\rho_e}\right)^2 \epsilon \tag{19}$$

Substituting equation (19) into equation (9) yields the following momentum equation:

$$\left(\overline{C}_1 f_{\eta\eta}\right)_\eta + (fD_2 + 2\overline{S}f_{\overline{S}})f_{\eta\eta} = 2\overline{S}f_\eta\left(f_\eta\right)_{\overline{S}} - \beta\left[\frac{1}{\frac{\rho}{\rho_e}} - (f_\eta)^2\right] \tag{20}$$

Multiplying the momentum equation (20) by the velocity gradient parameter β, which is constant across the boundary layer, gives

$$\left(\beta\overline{C}_1 f_{\eta\eta}\right)_\eta + (fD_2 + 2\overline{S}f_{\overline{S}})\beta f_{\eta\eta} = \beta 2\overline{S}f_\eta\left(f_\eta\right)_{\overline{S}} - \beta^2\left[\frac{1}{\frac{\rho}{\rho_e}} - (f_\eta)^2\right] \tag{21}$$

Now the momentum equation (21) has the proper form such that the following new dependent variable transformation can be used:

$$\mathscr{P} = \beta\overline{C}_1 f_{\eta\eta} \tag{22}$$

This substitution (eq. (22)) eliminates the need for numerically differentiating the eddy diffusivity. And more importantly, this transformation is believed to be an important factor in stabilizing the numerical boundary-layer solutions, especially for the adverse pressure gradients approaching flow separation and beyond.

When equation (22) is substituted into equation (21), the momentum equation in terms of the new dependent variable $\mathscr{P}$ has the form of an ordinary differential equation

$$\mathscr{P}_\eta + a\mathscr{P} = h \tag{23}$$

where

$$a = \frac{fD_2 + 2\bar{S}f_{\bar{S}}}{\bar{C}_1} \tag{24}$$

$$h = \beta 2\bar{S}f_\eta\left(f_\eta\right)_{\bar{S}} - \beta^2\left[\frac{1}{\frac{\rho}{\rho_e}} - \left(f_\eta\right)^2\right] \tag{25}$$

The following boundary conditions are applied to the momentum equation (23):

$$\left.\begin{aligned} f = f_\eta = 0 \quad &\text{at } \eta = 0 \\ f_\eta = 1.0 \quad &\text{at } \eta = \eta_e \end{aligned}\right\} \tag{26}$$

The nonsimilar streamwise velocity derivatives ($f_{\bar{S}}$ and $\left(f_\eta\right)_{\bar{S}}$) in equations (24) and (25) are evaluated with a simple two-point numerical derivative formulation. This simple formulation of the streamwise velocity derivatives reduces the momentum equation (23) to a linear, ordinary, differential equation (function of η only) and is easily integrated in closed form. The detailed numerical calculation method is given in appendix B.

Skin-Friction Coefficient and Boundary-Layer Thicknesses

The following definitions of various boundary-layer terms are useful for analyzing the behavior of the boundary layer, as well as for comparison with experimental data: The shear-stress distribution across the boundary layer is expressed as

$$\tau = (\mu + \rho\epsilon)\frac{\partial U}{\partial y} \tag{27}$$

When equations (8), (19), and (22) are substituted into equation (27), the nondimensional shear-stress function becomes

$$\frac{\mathscr{P}}{\beta} = \frac{\tau}{\left[\left(\frac{\rho_0\mu_0}{2\bar{S}}\right)^{1/2} U_e^{3/2}\right]} \tag{28}$$

From equation (28) the shear-stress function $\mathscr{P}$ is shown to be the nondimensional shear-stress distribution across the boundary layer. At the wall, the shear stress reduces to

$$\tau_w = \mu_w (U_y)_w = \frac{1}{2} \rho_e U_e^2 C_f \tag{29}$$

Substituting the transformation equations (8) into equation (29) and solving for the skin-friction coefficient C_f give

$$C_f = \frac{2}{\rho_e} \left(\frac{\rho_0 \mu_0}{U_e 2\bar{S}} \right)^{1/2} (Cf_{\eta\eta})_w \tag{30}$$

The following boundary-layer thicknesses are very useful for comparison with experimental measurements and other theoretical analyses:

Thickness	Definition	Transformed
Momentum	$\theta = \int_0^{y_e} \frac{\rho U}{\rho_e U_e} \left(1 - \frac{U}{U_e}\right) dy$	$\theta = \left(\frac{\rho_0 \mu_0 2\bar{S}}{U_e}\right)^{1/2} \frac{1}{\rho_e} \int_0^{\eta_e} f_\eta (1 - f_\eta)\, d\eta$
Displacement	$\delta^* = \int_0^{y_e} \left(1 - \frac{\rho U}{\rho_e U_e}\right) dy$	$\delta^* = \left(\frac{\rho_0 \mu_0 2\bar{S}}{U_e}\right)^{1/2} \frac{1}{\rho_e} \int_0^{\eta_e} \left(\frac{1}{\frac{\rho}{\rho_e}} - f_\eta\right) d\eta$

TURBULENT REYNOLDS SHEAR-STRESS MODEL

Before a comparison of the present theory with experimental data is made, a description of the present turbulent Reynolds shear-stress model and how it differs from other theoretical analyses is helpful. Most theoretical analyses use the eddy-diffusivity concept which states that the turbulent Reynolds shear stress is equal to the eddy diffusivity times the velocity gradient across the boundary layer.

Several analyses such as references 2, 3, and 6 use Prandtl's mixing-length theory with viscous damping near the wall matched to an outer constant eddy-diffusivity (wake) region. A slightly different eddy-diffusivity model, as in reference 5, consists of Prandtl's mixing-length eddy diffusivity for the entire boundary layer (like eq. (5)) but

with two different mixing-length regions. The first mixing-length region of reference 5 is Prandtl's classic mixing-length expression ($l = \kappa y$), and the second region is a constant approximated from experimental data, as shown in figure 2. The measured, nondimensioned, mixing length l/δ greatly increases near the edge of the boundary layer for low free-stream turbulence levels in adverse-pressure-gradient flows (refs. 14 and 15). However, the mixing length in reference 5 was assumed to be a constant in this region of the boundary layer.

Figure 3 gives a generally good comparison of Prandtl's mixing length with the general trend of the measured mixing length (ref. 9) for flows with high free-stream turbulence levels. Because of this favorable comparison of Prandtl mixing-length theory with data and the fact that flows with high free-stream turbulence levels generally occur over compressor blades, Prandtl's mixing-length theory is used for the eddy-diffusivity model in the present analysis.

COMPARISON OF PRESENT THEORY WITH EXPERIMENTAL MEASUREMENTS

The present turbulent-boundary-layer analysis was compared with the experimental boundary-layer data of reference 12 for a straight cascade at several inlet-flow angles. The cascade of reference 12 consisted of nine blades with a chord length of 12.4 centimeters, a span of 50.8 centimeters, and an NACA 65-410 airfoil section. The free-stream flow properties were calculated from the static-pressure measurements along the airfoil that are presented in reference 12. The boundary-layer measurements on the cascade airfoil were compared with the present analysis for the following three different inlet-flow conditions:

(1) Two-dimensional flow with a cascade inlet-flow angle of 55° (2D-55°)

(2) Two-dimensional flow with a cascade inlet-flow angle of 65° (2D-65°)

(3) Three-dimensional flow with a cascade inlet-flow angle of 60° (3D-60°)

In the third flow condition (3D-60°), three-dimensional flow was simulated by producing an added velocity diffusion near one end of the cascade blades. (Although the present analysis is strictly a two-dimensional analysis, the present calculation system was still applied to this simulated three-dimensional flow.) The added velocity diffusion was artificially produced by placing an obstruction downstream of the span-wise centerline of the cascade (ref. 11). The turbulence intensity level for this cascade is reported to be high (ref. 12). For all inlet-flow conditions, the flow over the cascade blades is incompressible.

Boundary-Layer Thicknesses

In figures 4 and 5 the predicted momentum and displacement thicknesses along the airfoil section are compared with experimental data (ref. 12) for the three cascade inlet-flow conditions. In general, the predicted momentum and displacement thickness distributions along the airfoil are in favorable agreement with the experimental data.

For the suction surface with the inlet-flow condition 2D-55°, the greatest discrepancy (10 to 20 percent) between the predicted and measured thicknesses occurred at 80 and 90 percent of chord (fig. 4(a)). This discrepancy is believed to result partially from an inaccurate velocity gradient β distribution along the airfoil. Since the boundary-layer growth is a strong function of β, any error in β will significantly affect the boundary-layer thicknesses. The calculation of β involves a numerical differentiation of an experimentally determined free-stream velocity distribution. Thereby, two sources of error are apparent: the reduction of experimental pressure measurements to a velocity distribution and the numerical differentiation of this velocity distribution. In addition, reference 12 presents the pressure measurements in graphical form without a grid, which necessitates an interpolation of measured results - another source of error.

Figure 4(b), for the pressure surface 2D-55°, shows that the predicted thicknesses reduced more rapidly than measured values as the favorable pressure gradient was encountered at the last 25 percent of the chord. Again, this difference between the predicted and measured thicknesses is believed to be caused primarily by an inaccurate distribution of β along the airfoil.

Although the turbulent boundary layer separated on the suction surface for inlet-flow conditions of 2D-65° and 3D-60°, the predicted thicknesses still compared favorably with measured values (figs. 5(a) and (b)). The distribution of the predicted skin-friction coefficient along the suction surface is also given in figures 5(a) and (b). The point on the airfoil surface at which the skin-friction coefficient first becomes negative is a good indication of the location of boundary-layer separation. Figures 5(a) and (b) show that the turbulent boundary layer separated at about 70 percent of chord for the inlet-flow condition 2D-65° and at approximately 40 percent of chord for the inlet-flow condition 3D-60°.

Velocity Profiles

In figures 6 to 9 the predicted velocity profiles are compared with experimental data for the three cascade inlet-flow conditions at 20 or 98 percent of chord. These velocity profiles are presented as a function of the transformation variable η, which is

independent of the skin-friction coefficient. Usually, the velocity profile is presented as a function of a wall distance variable y^+ (ref. 16), which requires a knowledge of the skin-friction coefficient. Since η does not depend upon the skin-friction coefficient, the present comparison of predicted velocity profiles with experiment data does not contain any error from the experimental or predicted skin-friction coefficients. Also, near the separated region the skin-friction coefficient becomes very small and experimentally susceptible to large errors (if determinable at all).

For the first cascade inlet-flow condition (2D-55°), the predicted velocity profile at 20 percent of chord is in excellent agreement with the limited experimental data (fig. 6). Even at 98 percent of chord, the predicted velocity profile is still in good agreement with experimental data (fig. 7) for the same inlet-flow condition (2D-55°). For a higher cascade inlet-flow angle (2D-65°) with increased velocity diffusion, figure 8 shows good agreement of the predicted velocity profile with experimental data at 98 percent of chord. Similarly, for even larger velocity diffusion (3D-60°), the predicted velocity profile is still in good agreement with experimental data at 98 percent of chord (fig. 9). This good comparison of the predicted with the experimental velocity profiles shown in figures 8 and 9 is of special interest because the turbulent boundary layer had already separated upstream of the 98-percent-of-chord station. In fact, for the largest velocity diffusion case (3D-60°), the predicted turbulent-boundary-layer separation point occurred at approximately 40 percent of chord. Therefore, the present turbulent-boundary-layer theory is shown to predict accurate velocity profiles and thereby accurate boundary-layer thicknesses, even for a significantly separated turbulent boundary layer on this particular cascade blade. However, the present theory has thus far only been applied to this one set of cascade data for a separated, turbulent, boundary layer. Additional separated-boundary-layer data over a wider range of flow conditions are needed to assess the accuracy, generality, and applicability to different flow orientations of the present analysis.

CONCLUSIONS

In order to provide an approximate boundary-layer prediction at the trailing edge of a compressor blade (especially with separated flow), a two-dimensional differential analysis was developed for the turbulent boundary layer (including the separated reverse-flow region). The use of a new shear-stress function (instead of a velocity function) for the dependent variable in the momentum equation made it possible to calculate mathematically stable solutions into the boundary-layer separation region. Prandtl's classical mixing-length theory was used with a single eddy-diffusivity model throughout the boundary-layer region.

This analysis was applied to a blade in a cascade with three different inlet-flow angles for comparison with existing experimental boundary-layer measurements. The predicted turbulent-boundary-layer thicknesses and velocity profiles are in good agreement with experimental data, even in the separated region. For the thickest turbulent boundary layer on the blade with a separated region, 8 minutes of computing time (Lewis DCS 7094-7044) are necessary for this calculation.

Lewis Research Center,
National Aeronautics and Space Administration,
Cleveland, Ohio, December 20, 1973,
501-24.

APPENDIX A

SYMBOLS

A	constant, eq. (6)
a	term in momentum equation, eq. (24)
C	density-viscosity ratio, eq. (11)
C_f	skin-friction coefficient, eq. (30)
$\overline{C}_1$	transformation parameter, eq. (19)
c	chord length
c_p	specific heat at constant pressure
D_1	flow coefficient, eq. (14)
D_2	flow coefficient, eq. (15)
D_3	flow coefficient, eq. (12)
$\frac{dU_e}{dS}$	velocity derivative at edge of boundary layer
e	natural or Naperian base ($e = 2.71828$)
f	velocity ratio, U/U_e
H	total enthalpy
h	term in momentum equation, eq. (25)
I_Q	iteration criterion, eq. (B16)
K_1	constant of integration, eq. (B15)
K_2	constant of integration ($K_2 = 0$)
K_3	constant of integration ($K_3 = 0$)
l	mixing length
P	static pressure
$\mathscr{P}$	dependent variable transformation, eq. (22)
Pr_L	laminar Prandtl number
Pr_T	turbulent Prandtl number
$\mathfrak{R}$	universal gas constant
$\overline{S}$	boundary-layer coordinate parallel to blade surface, $\overline{S} = S$

T	total temperature
t	static temperature
U	velocity parallel to blade surface
V	velocity normal to blade surface
x	distance coordinate from nose to trailing edge of airfoil section
y	boundary-layer coordinate normal to blade surface
y^+	wall distance parameter, eq. (18)
β	velocity gradient parameter, eq. (16)
δ	boundary-layer thickness
δ^*	displacement thickness
ϵ	eddy diffusivity
η	transformed coordinate in y-direction, eq. (8a)
θ	momentum thickness
κ	empirical constant (0.40)
μ	molecular viscosity
ρ	density
τ	shear stress
ψ	stream function
ω	integration factor, eq. (B11)

Subscripts:

e	edge of boundary-layer condition
Q	iteration number (increase in η_e)
w	wall condition
y, yy	derivatives of function with respect to y or $\bar{S}$ coordinate
$\eta, \eta\eta$	derivatives of function with respect to the transformed η coordinate
0	reference stagnation condition

Superscript:

d	exponent for viscosity variation with temperature (0.65 for air)

APPENDIX B

CALCULATION PROCEDURE

For ease of reference, the transformed momentum-boundary-layer equation and the boundary conditions are repeated here.

$$\mathscr{P}_{\eta} + a\mathscr{P} = h \tag{B1}$$

where

$$a = \frac{fD_2 + 2\bar{S}f_{\bar{S}}}{\bar{C}_1} \tag{B2}$$

$$h = \beta 2\bar{S}f_{\eta}(f_{\eta})_{\bar{S}} - \beta^2\left[\frac{1}{\frac{\rho}{\rho_e}} - (f_{\eta})^2\right] \tag{B3}$$

with the boundary conditions

$$f = f_{\eta} = 0 \quad \text{at} \quad \eta = 0 \tag{B4}$$

$$f_{\eta} = 1.0 \quad \text{at} \quad \eta = \eta_e \tag{B5}$$

where η_e is the boundary-layer thickness in the transformed η-coordinate.

The nonsimilar streamwise derivatives $f_{\bar{S}}$ and $(f_{\eta})_{\bar{S}}$ are approximated in the following manner:

$$f_{\bar{S}} = \frac{f - f_{\bar{S}-1}}{\Delta\bar{S}} \tag{B6}$$

$$(f_{\eta})_{\bar{S}} = \frac{(f_{\eta})_{\bar{S}} - (f_{\eta})_{\bar{S}-1}}{\Delta\bar{S}} \tag{B7}$$

where $f_{\bar{S}-1}$ and $(f_\eta)_{\bar{S}-1}$ are the velocity functions at the previous $\bar{S}$ location. The nonsimilar derivatives are underrelaxed as follows:

$$(f_{\bar{S}})_R = (f_{\bar{S}})_{\bar{S}-1} + 0.1\left[f_{\bar{S}} - (f_{\bar{S}})_{\bar{S}-1}\right] \tag{B8}$$

$$\left[(f_\eta)_{\bar{S}}\right]_R = (f_\eta)_{\bar{S}-1} + 0.1\left[(f_\eta)_{\bar{S}} - (f_\eta)_{\bar{S}-1}\right] \tag{B9}$$

where the subscript R denotes relaxed derivatives.

Solution of Momentum Equation

The simple two-point formulation of the streamwise velocity derivatives, equations (B6) and (B7), reduce the momentum equation (B1) to a linear, ordinary, differential equation (function of η only). This linear, ordinary, differential equation (B1) of the first order can readily be solved in the following manner:

$$\mathscr{P} = \frac{1}{\omega}\int_0^\eta \omega h \, d\eta + \frac{K_1}{\omega} \tag{B10}$$

where

$$\omega = \exp\left(\int_0^\eta a \, d\eta\right) \tag{B11}$$

and

$$f_{\eta\eta} = \frac{\mathscr{P}}{\bar{C}_1\beta} \tag{B12}$$

$$f_\eta = \int_0^\eta f_{\eta\eta} \, d\eta + K_2 \tag{B13}$$

$$f = \int_0^\eta f_\eta \, d\eta + K_3 \tag{B14}$$

When the boundary conditions (B4) and (B5) are applied to equations (B10) to (B14), the constants of integration (K_1, K_2, K_3) become

$$K_2 = K_3 = 0$$

$$K_1 = \frac{\beta - \int_0^{\eta_e} \frac{1}{\omega \bar{C}_1} \left(\int_0^{\eta} \omega h \, d\eta \right) d\eta}{\int_0^{\eta_e} \frac{d\eta}{\omega \bar{C}_1}} \tag{B15}$$

The general procedure for determining the edge of the boundary layer (correct η_e) is to compare the velocity derivative at the wall $(f_{\eta\eta})_w$ between successive increments in η_e. If the iteration criterion for the change in $(f_{\eta\eta})_w$ is met, the edge of the boundary layer is obtained. In detail, the correct η_e is determined by the following iteration procedure:

(1) Assume some initial η_e and increase η_e by $\Delta\eta_e$ for each outer iteration.

(2) Use the following iteration criterion: Let

$$I_Q = \frac{\left[(f_{\eta\eta})_w \right]_{Q+1} - \left[(f_{\eta\eta})_w \right]_Q}{\left[(f_{\eta\eta})_w \right]_{Q+1}} \tag{B16}$$

where Q indicates the iteration number (increase in η_e). If $|I_Q| < 0.005$, the correct η_e and boundary-layer solution are obtained.

General Flow of Program

The general flow of the program is as follows:

(1) Input the total flow conditions (P_0, T_0, μ_0, etc.) and the table of $\bar{S}$ against P_e/P_0.

(2) For a given distribution of $\bar{S}$ (interval in $\bar{S}$), calculate all free-stream conditions, such as β, D_2, ρ_e, D_3, U_e, and D_1.

(3) For the initial η_e and the initial iteration of the first $\bar{S}$, estimate the starting

profiles of f_η and $f_{\eta\eta}$ with a 1/7 power law and neglect nonsimilar terms.

(4) Calculate the coefficients a_η and h_η.

(5) Solve equations (B6) to (B10) to obtain a new approximation for f_η and $f_{\eta\eta}$.

(6) Iterate steps 4 and 5 until the magnitudes of a (eq. (B2)) are approximately equal from successive iterations (maximum of four iterations).

(7) Check I_Q to see if $|I_Q| < 0.005$.

(8) If $|I_Q| > 0.005$, increase η_e by $\Delta\eta_e$ and go to step 4.

(9) If $|I_Q| < 0.005$, the boundary-layer profiles, thicknesses, and important parameters are printed out and the program proceeds to the next $\bar{S}$ (step 2).

REFERENCES

1. McNally, William D.: FORTRAN Program for Calculating Compressible Laminar and Turbulent Boundary Layers in Arbitrary Pressure Gradients. NASA TN D-5681, 1970.

2. Smith, A. M. O.; and Cebeci, T.: Numerical Solution of the Turbulent-Boundary-Layer Equations. Rep. DAC-33735, Douglas Aircraft Co., Inc., May 29, 1967. (Available from DDC as AD-656430.)

3. Herring, H. James; and Mellor, George L.: A Method of Calculating Compressible Turbulent Boundary Layers. NASA CR-1144, 1968.

4. Patanker, S. V.; and Spalding, D. B.: Heat and Mass Transfer in Boundary Layers. International Textbook, 1968.

5. Bushnell, Dennis M.; and Beckwith, Ivan E.: Calculation of Nonequilibrium Hypersonic Turbulent Boundary Layers and Comparisons with Experimental Data. AIAA J., vol. 8, No. 8, Aug. 1970, pp. 1462-1469.

6. Harris, Julius E.: Numerical Solution of the Equations for Compressible Laminar, Transitional, and Turbulent Boundary Layers and Comparisons with Experimental Data. NASA TR R-368, 1971.

7. Kuhn, Gary D.; and Nielsen, Jack N.: An Analytical Method for Calculating Turbulent Separated Flows Due to Adverse Pressure Gradients. SQUID-TR-NEAR-1-PU, Purdue Univ. (AD-731744), 1971.

8. Schmidt, James F.; Boldman, Donald R.; and Todd, Carroll: Similar Solutions for Turbulent Boundary Layer with Large Favorable Pressure Gradients (Nozzle Flow with Heat Transfer). NASA TN D-6439, 1971.

9. Schlichting, Hermann (J. Kestin, trans.): Boundary Layer Theory. Second ed., McGraw-Hill Book Co., Inc., 1955.

10. Huffman, David G.; Zimmerman, D. R.; and Bennett, W. A.: The Effect of Free Stream Turbulence Level on Turbulent Boundary Layer Behaviour. Boundary Layer Effects in Turbomachines. J. Surugue, ed., AGARD-AG-164, 1972, pp. 89-115.

11. Van Driest, E. R.: On Turbulent Flow Near A Wall. Jour. Aeron. Sci., vol. 23, no. 11, Nov. 1956, pp. 1007-1011.

12. Peterson, Carl R.: Boundary Layer on an Airfoil in a Cascade. Rep. No. 49, Gas Turbine Laboratory, M.I.T., Dec. 1958.

13. Smith, A. M. O.; and Clutter, Darwin W.: Machine Calculation of Compressible Laminar Boundary Layers. AIAA Jour., vol. 3, no. 4, April, 1965, pp. 639-647.

14. Bradshaw, P.; and Ferriss, D. H.: The Response of a Retared Equilibrium Turbulent Boundary Layer to the Sudden Removal of Pressure Gradient. NPL-AERO-1145; ARC-26758, National Physical Laboratory, Aerodynamics Division, May 1965.

15. Escudier, M. P.; and Spalding, D. B.: A Note on the Turbulent Uniform-Property Hydrodynamic Boundary Layer on a Smooth Impermeable Wall; Comparisons of Theory with Experiment. ARC-CP-875; ARC-27302, Aeronautical Research Council, Aug. 1965.

16. Deissler, R. G.; and Loeffler, A. L., Jr.: Analysis of Turbulent Flow and Heat Transfer on a Flat Plate at High Mach Numbers with Variable Fluid Properties. NASA TR R-17, 1959.

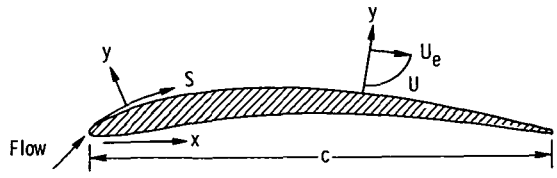

Figure 1. - Boundary-layer coordinate system along blade cross section.

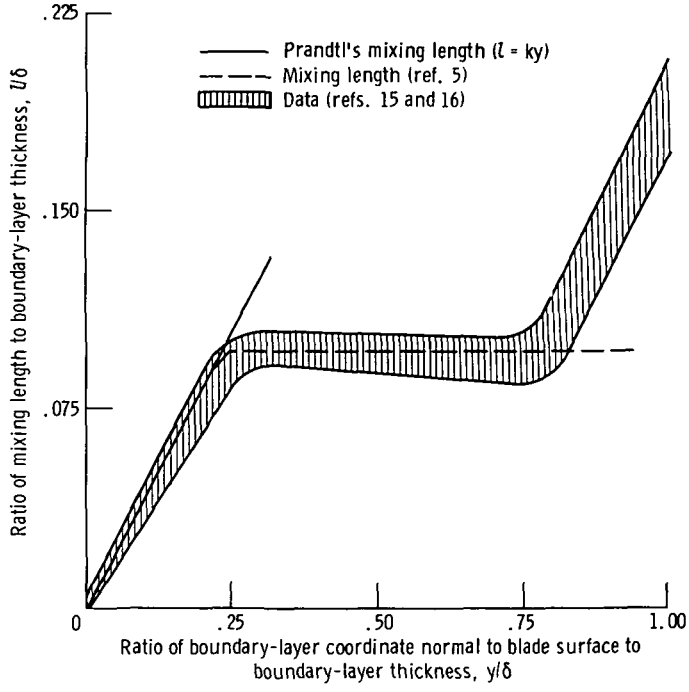

Figure 2. - Approximate comparison of measured mixing length with Prandtl's mixing length for low free-stream turbulence levels.

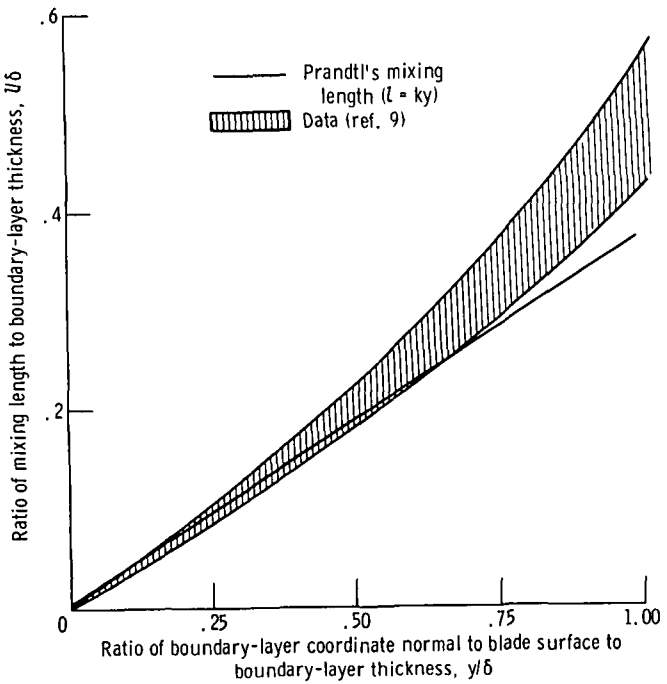

Figure 3. - Approximate comparison of measured mixing length with Prandtl's mixing length for high free-stream turbulence levels.

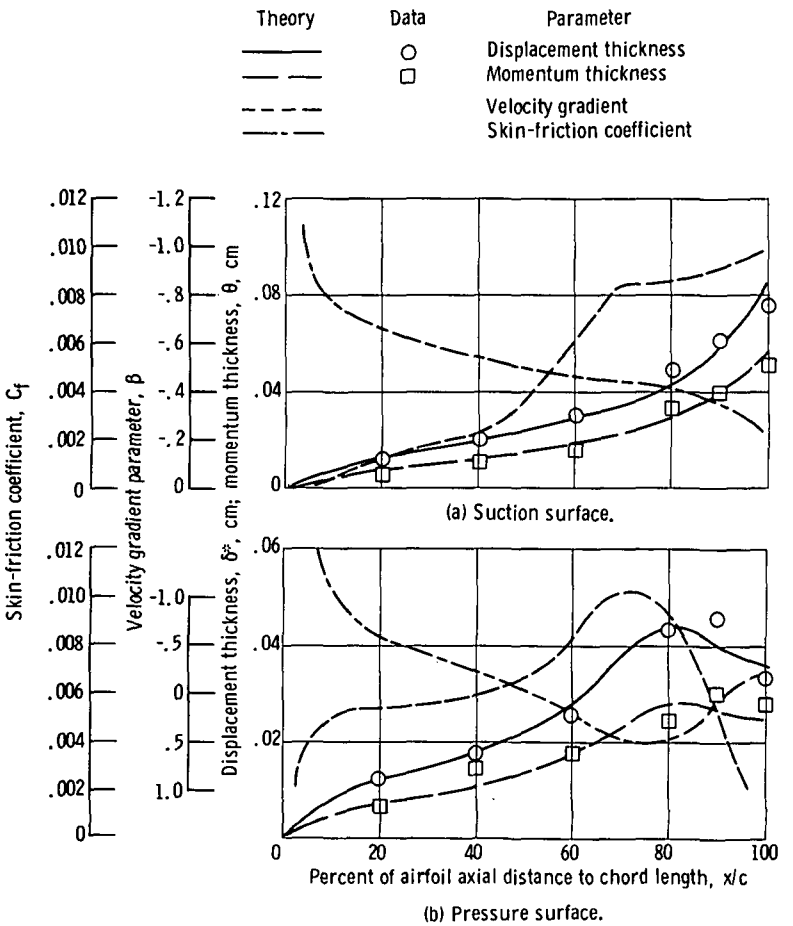

Figure 4. - Comparison of predicted displacement and momentum thicknesses with experimental data (ref. 12) along the cascade airfoil section for two-dimensional flow with a cascade inlet-flow angle of 55^0 (2D-55^0).

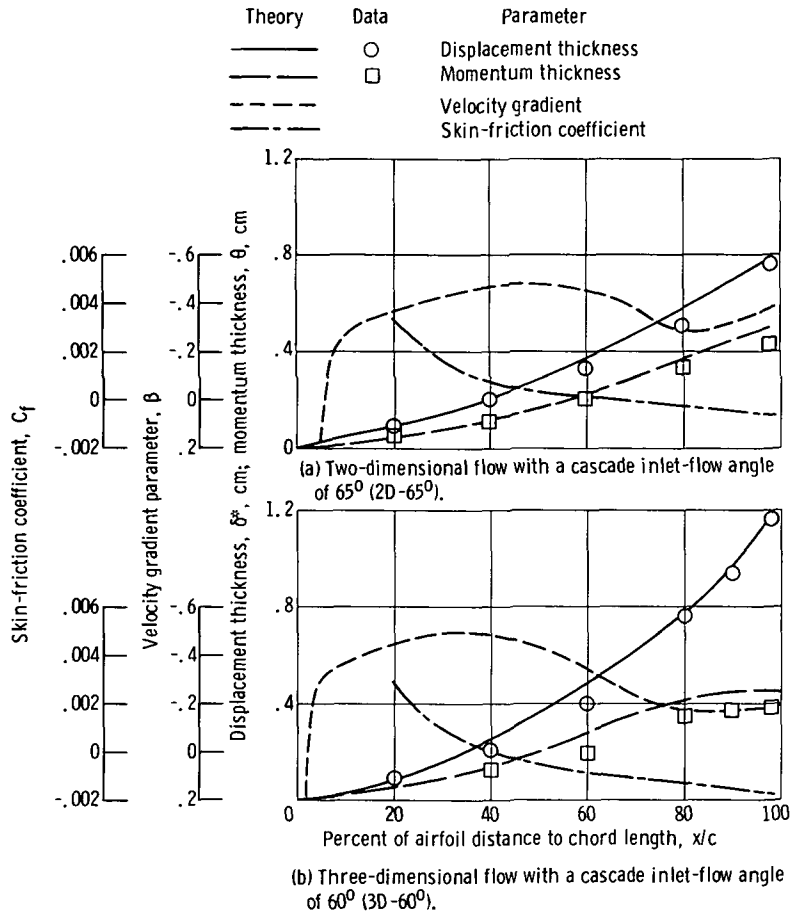

(a) Two-dimensional flow with a cascade inlet-flow angle of 65^0 ($2D\text{-}65^0$).

(b) Three-dimensional flow with a cascade inlet-flow angle of 60^0 ($3D\text{-}60^0$).

Figure 5. - Comparison of predicted displacement and momentum thicknesses with experimental data (ref. 12) along the suction surface of the cascade airfoil section for two inlet-flow conditions.

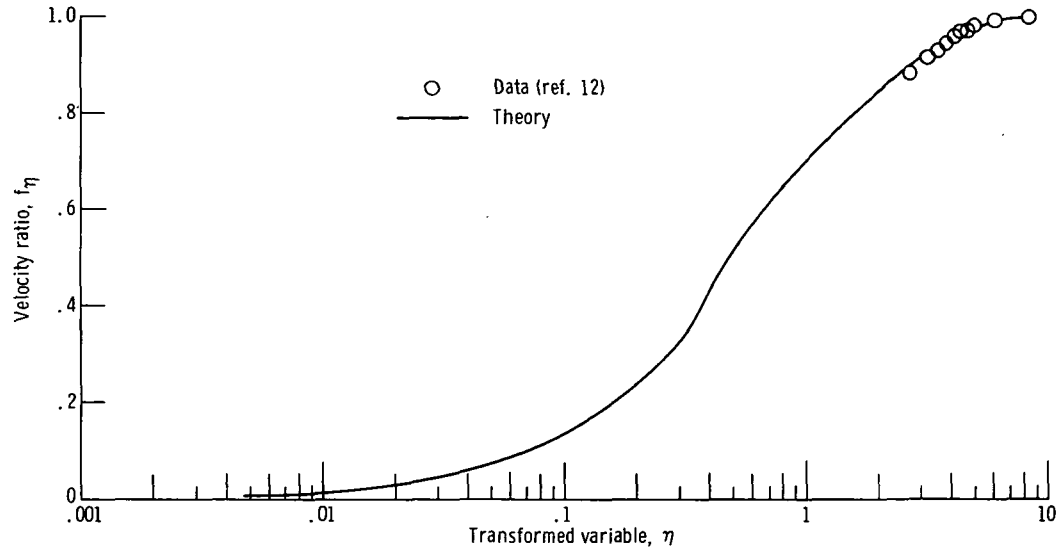

Figure 6. - Comparison of predicted velocity profile with experimental data at 20 percent of chord for two-dimensional flow on the suction surface at a inlet-flow angle of 55°.

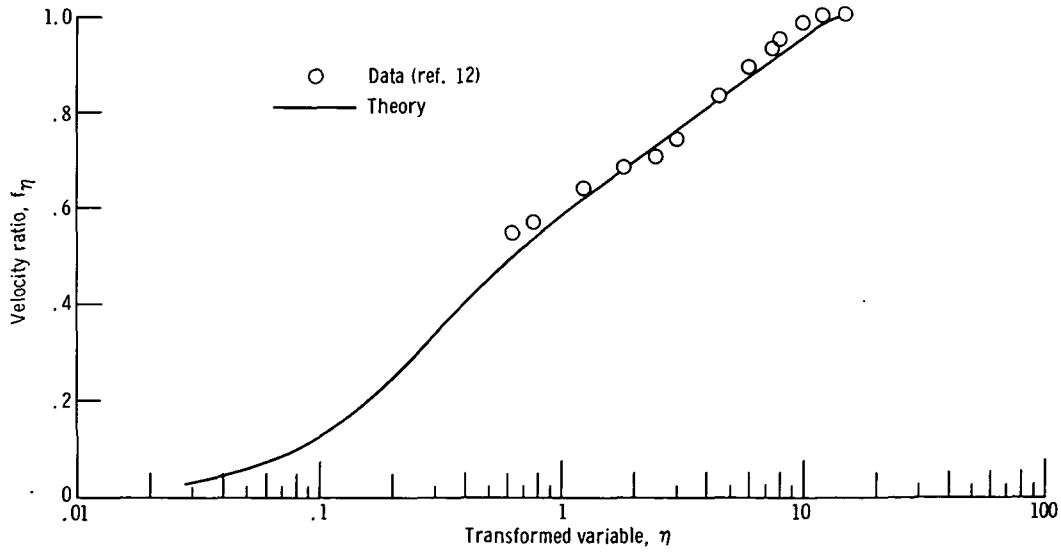

Figure 7. - Comparison of predicted velocity profile with experimental data at 98 percent of chord for two-dimensional flow on the suction surface at an inlet-flow angle of 55°.

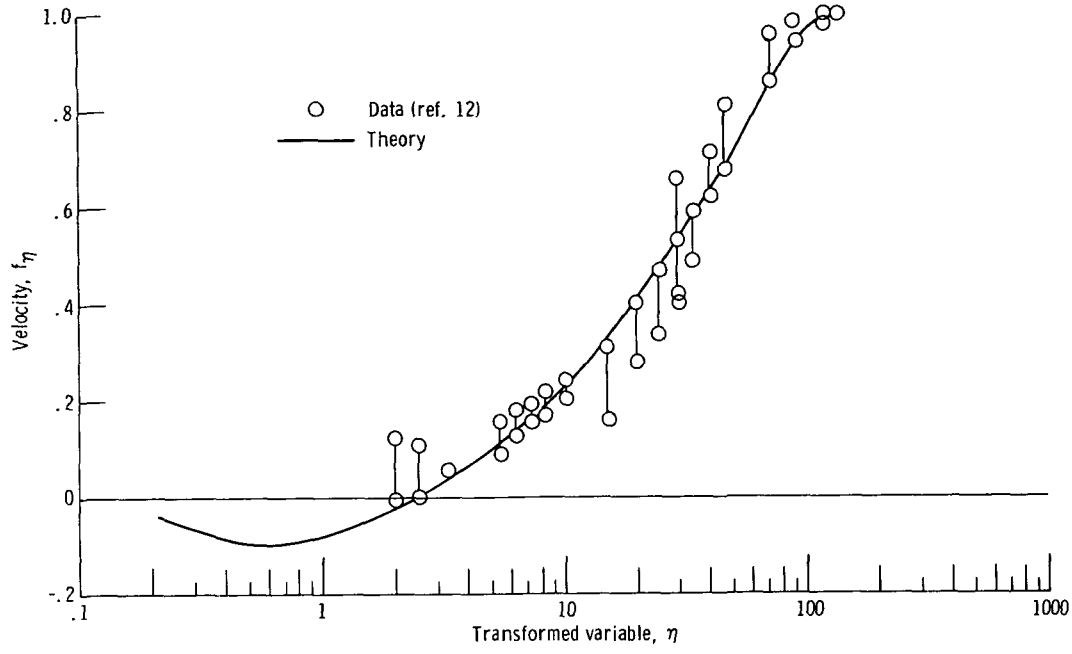

Figure 8. - Comparison of predicted velocity profile with experimental data at 98 percent of chord for two-dimensional flow on the suction surface at an inlet-flow angle of 65^0.

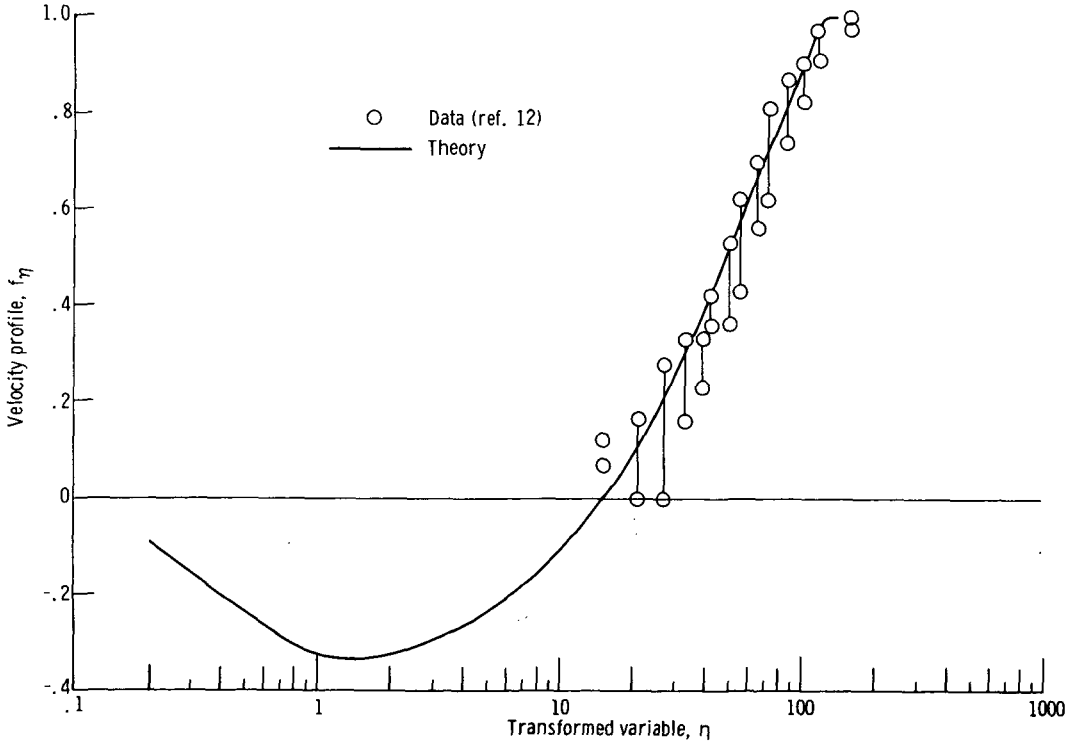

Figure 9. - Comparison of predicted velocity profile with experimental data at 98 percent of chord for three-dimensional flow on the suction surface at an inlet-flow angle of 60^0.

Page Intentionally Left Blank

"The aeronautical and space activities of the United States shall be conducted so as to contribute . . . to the expansion of human knowledge of phenomena in the atmosphere and space. The Administration shall provide for the widest practicable and appropriate dissemination of information concerning its activities and the results thereof."

—NATIONAL AERONAUTICS AND SPACE ACT OF 1958

NASA SCIENTIFIC AND TECHNICAL PUBLICATIONS

TECHNICAL REPORTS: Scientific and technical information considered important, complete, and a lasting contribution to existing knowledge.

TECHNICAL NOTES: Information less broad in scope but nevertheless of importance as a contribution to existing knowledge.

TECHNICAL MEMORANDUMS: Information receiving limited distribution because of preliminary data, security classification, or other reasons. Also includes conference proceedings with either limited or unlimited distribution.

CONTRACTOR REPORTS: Scientific and technical information generated under a NASA contract or grant and considered an important contribution to existing knowledge.

TECHNICAL TRANSLATIONS: Information published in a foreign language considered to merit NASA distribution in English.

SPECIAL PUBLICATIONS: Information derived from or of value to NASA activities. Publications include final reports of major projects, monographs, data compilations, handbooks, sourcebooks, and special bibliographies.

TECHNOLOGY UTILIZATION PUBLICATIONS: Information on technology used by NASA that may be of particular interest in commercial and other non-aerospace applications. Publications include Tech Briefs, Technology Utilization Reports and Technology Surveys.

Details on the availability of these publications may be obtained from:

SCIENTIFIC AND TECHNICAL INFORMATION OFFICE

NATIONAL AERONAUTICS AND SPACE ADMINISTRATION

Washington, D.C. 20546